Nuclear Materials and Energy 12 (2017) 1071–1076

Contents lists available at ScienceDirect

Nuclear Materials and Energy

journal homepage: www.elsevier.com/locate/nme

Detachment evolution on the TCV tokamak

J.R. Harrison[a,*], W.A.J. Vijvers[b], C. Theiler[c], B.P. Duval[c], S. Elmore[a], B. Labit[c], B. Lipschultz[d], S.H.M. van Limpt[b], S.W. Lisgo[e], C.K. Tsui[c,f], H. Reimerdes[c], U. Sheikh[c], K.H.A. Verhaegh[c,d], M. Wischmeier[g], the MST1 and TCV Teams

[a] CCFE, Culham Science Centre, Abingdon, OX14 3DB, Oxon UK
[b] FOM Institute DIFFER, Dutch Institute for Fundamental Energy Research, The Netherlands
[c] Ecole Polytechnique Fédérale de Lausanne (EPFL), SPC, 1015 Lausanne, Switzerland
[d] York Plasma Institute, Department of Physics, University of York, Heslington, York, YO10 5DD, UK
[e] ITER Organization, Route de Vinon-sur-Verdon, St.Paul-lez-Durance, Cedex, France
[f] University of California San Diego (UCSD), San Diego, CA, USA
[g] Max Planck Institut für Plasmaphysik, Boltzmannstr. 2, 85748 Garching, Germany

ARTICLE INFO

Article history:
Received 15 July 2016
Revised 29 September 2016
Accepted 17 October 2016
Available online 24 December 2016

ABSTRACT

Divertor detachment in the TCV tokamak has been investigated through experiments and modelling. Density ramp experiments were carried out in ohmic heated L-mode pulses with the ion ∇B drift directed away from the primary X-point, similar to previous studies [1]. Before the roll-over in the ion current to the outer strike point, C III and D_α emission from the outer leg recede slowly from the strike point toward the X-point, at a rate of $\sim 2.0 \times 10^{-19}$ m/m^{-3} along the magnetic field as the electron temperature along the leg reduces with increasing density. Around the onset of detachment, the upstream density profile and outer target D_α profiles broaden, possibly leading to an increase in radiation in the SOL by increased interaction between the SOL and the carbon tiles lining the outer wall. The plasma conditions upstream and at various locations along the detached outer divertor leg have been characterised, and the consistency of this data has been checked with the interpretive OSM-EIRENE-DIVIMP suite of codes [2] and are broadly found to be consistent with measured D_γ/D_α emissivity profiles along the detached outer divertor leg.

1. Introduction

Divertor detachment has been demonstrated to mitigate the steady-state heat flux to divertor plasma-facing components in several magnetic confinement fusion devices ([3–7] and references therein), and will likely be a necessary prerequisite for the operation of larger scale devices such as ITER and DEMO. Physics studies of divertor detachment have been carried out on the TCV tokamak, with unparalleled flexibility to produce a range of magnetic configurations and in an open divertor geometry allowing excellent access for diagnostics. Recent experiments were carried out to build on previous studies [1,8] to characterise the dynamic evolution of the plasma conditions in the divertor and main chamber during the onset and evolution of detachment, and to check the consistency of the data with interpretive modelling tools. This provides a basis for comparison with alternative divertor configurations, such as the snowflake [9], Super-X or X-point target [10,11], and provides more insight into the processes governing detachment in TCV.

Density ramp experiments were carried out in L-mode ohmic heated discharges in the lower single null configuration, $I_p = 340$kA, $q_{95} = 2.5$, $B_\varphi = 1.43$T, with the ion ∇B drift directed away from the primary X-point in order to elevate the power threshold for the L-mode to H-mode transition. One density ramp experiment is studied in detail here, shot 52,065, where the poloidal length of the inner and outer divertor legs was 10 cm and 40 cm respectively, and the poloidal flux expansion at the outer strike point was ~6. The evolution of the plasma parameters upstream and at the divertor targets is shown in Fig. 1. At the beginning of the density ramp, at a Greenwald fraction ($f_{GW} = \langle n_e \rangle (10^{20}\,\mathrm{m}^{-3})/(I_p\ (\mathrm{MA})/(\pi a^2\ (\mathrm{m}^2))$ of ~0.25 and collisionality ($\upsilon^*_e \sim 10^{-16}\ n_{e,u}\ (\mathrm{m}^{-3})\ L_{||}\ (\mathrm{m})\ /T_{e,u}{}^2\ (\mathrm{eV}^2)$) of ~15. The total ion flux to both inner and outer strike points, measured by Langmuir probes embedded in the divertor tiles, increases approximately linearly

* Corresponding author.
E-mail addresses: james.harrison@ukaea.uk, james.harrison@ccfe.ac.uk (J.R. Harrison).

http://dx.doi.org/10.1016/j.nme.2016.10.020

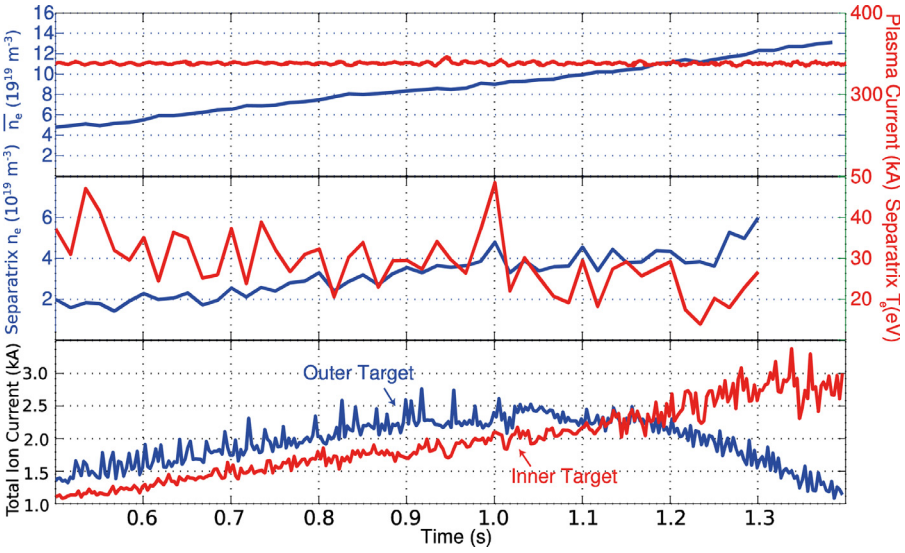

Fig. 1. Overview of the parameters of the shot under investigation, given by the plasma current and line average density measured with interferometry (top), the evolution of the upstream temperature and density estimated with Thomson scattering, (middle) and the evolution of the total ion flux to the inner and outer divertor targets (bottom).

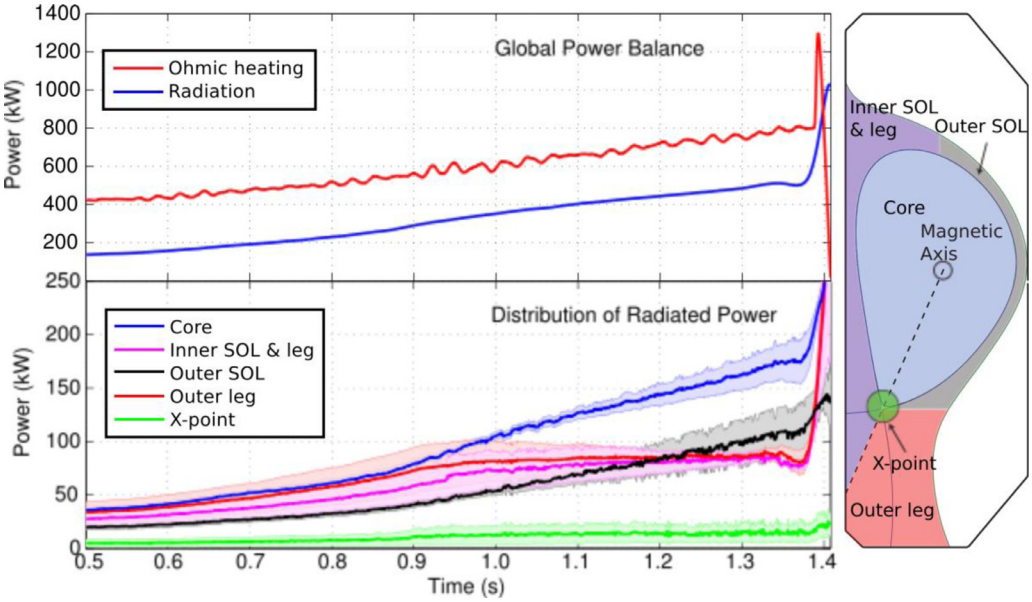

Fig. 2. (top) evolution of the ohmic heating power and radiative losses, (bottom) spatial distribution of the radiative losses, (right) the definitions of the regions associated with the radiated power curves in the bottom panel.

with the upstream density, until a roll-over occurs at the outer strike point at ~1 s ($f_{GW} \sim 0.48$, $\upsilon^*_e \sim 50$), and the flux to the inner strike point continues to increase until the end of the shot when the plasma disrupts, at $f_{GW} = 0.7$, $\upsilon^*_e \sim 100$.

In the upcoming sections, a detailed analysis of the experiment is presented in terms of power balance (Section 2), evolution of the profiles of temperature and density upstream, and the ion flux to the outer divertor strike point (Section 3), and the dynamic behaviour of the spectral line emission along the outer leg (Section 4). The consistency of the data presented are studied using the interpretive OSM-EIRENE DIVIMP suite of codes (Section 5), followed by conclusions (Section 6).

2. Power balance

Throughout the density ramp experiment, the ohmic heating power rises at a similar rate as the radiated power, estimated using gold foil bolometers, as shown in Fig. 2. Tomographic reconstructions of the poloidal distribution of the radiation were used to localise the radiation. Before the onset of detachment, the radiated power inside and outside the confined plasma increase as the density rises. After the roll-over in the total ion current at outer strike point, at ~1 s, the radiated power in both the inner and outer divertor legs stop increasing. In the case of the detached outer leg, the electron temperature continually decreases below ~10 eV. In these conditions, the radiation loss function of carbon, the strongest radiation source in TCV, decreases with decreasing temperature [12]. This leads to a contraction in the radiating volume in the outer divertor leg, and a concentration of radiation near the X-point. This observation has been made on several other devices when the divertor is deeply detached, such as JET [4], AUG [13]. Radiation in the outer SOL increases strongly before the roll-over, at ~0.9 s, possibly due to a broadening of the upstream density profile, as seen on AUG and other devices [14], resulting increased sputtering of impurities from carbon tiles lining the outer wall.

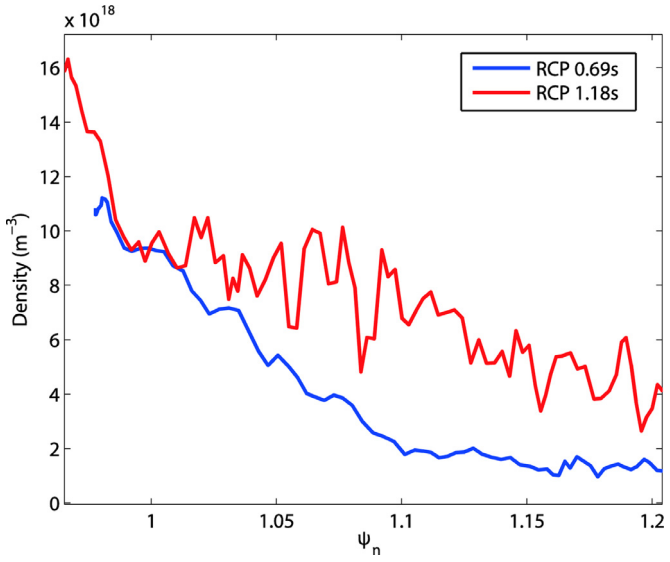

Fig. 3. Upstream density profiles plotted in terms of normalised flux, measured with a reciprocating probe before and after the onset of detachment. In the latter case, a 'shoulder' in the density profile has formed.

3. Profile evolution

The roll-over in the total ion current to the outer strike point, indicative of the onset of detachment, occurs due to a reduction of the ion flux in the vicinity of the separatrix; the peak ion current reduces by a factor of ~4 between the start of the roll-over and the end of the shot. The upstream and outer target electron density were measured with Thomson scattering and Langmuir probes respectively. Before the roll-over, the upstream and target densities are similar, and the target density rises approximately linearly with the upstream density. Measurements of the electron temperature at the same locations before the onset of detachment indicate that the temperature decreases by a factor of ~2 from upstream to the target, suggesting parallel heat conduction is playing a role in transporting heat to the divertor. The electron density at the outer strike point ceases to rise linearly with the upstream density after ~0.9 s and decreases strongly after ~1 s. This drop in density is stronger than the steady decrease in the target electron temperature throughout the density ramp, suggesting the reduction in density is largely responsible for the roll-over in the ion flux.

Measurements of the upstream density profiles with a reciprocating probe before and after the onset of detachment, shown in Fig. 3, indicate that the upstream density profile is broader after the onset of detachment, and the electron density near the outer wall increases by a factor ~3, which is consistent with probe measurements made in earlier experiments (not shown) that indicate that the ion flux to the wall increases linearly with the line average density. The increased plasma-surface interaction with the outer wall, and resulting sputtering of carbon from the tiles lining the wall, could explain the apparent increase in radiation in the outer SOL shown in Fig. 2. This possible explanation for the onset of detachment in TCV was previously investigated with SOLPS modelling [8], and was found to reconcile some discrepancies between the modelling and data from experiments.

4. Detachment dynamics

The MultiCam diagnostic was central to our studies of detachment evolution. Multicam uses beamsplitters to image 4 different spectral lines onto 4 different cameras simultaneously all with the same field of view of the divertor region. The filtered images are of D_α (656.1 nm), D_γ (434 nm), C II (426.7) and C III (465 nm). The 4 cameras operate at a 40 Hz frame rate and 640×480 resolution, viewing the lower half of the machine tangentially. The uncalibrated images were tomographically inverted to produce 2D emissivity profiles of the 4 spectral lines and their evolution through the density ramp. The data were inverted on a poloidal mesh of toroidally continuous volumes with a rectangular cross section with $\Delta r = 4$ mm and $\Delta z = 3.8$ mm. The inversions were calculated using an iterative SART algorithm with a non-negativity constraint [15].

The inverted Multicam images lead to a picture of detachment which can be characterized by fairly slow movement of the detached region and the underlying temperature profile. Inverted emissivities of D_α and C III lines calculated at 0.6 s, before the onset of detachment and at 1.0 s, during the onset, are shown in Fig. 4. The inversions indicate that before detachment, the peak of the D_α and CIII emission are peaked at the divertor strike points. At the onset of detachment, D_α emission is still most intense close to the divertor strike points, but has a larger radial width and is peaked away from the separatrix, as observed previously [1]. Also, at the onset of detachment, the C III emissivity is peaked near the X-point and extends to half way down the outer leg. Fig. 5 shows that both the D_α and C III emission recede from the strike point, starting with C III at 0.68 s, 0.32 s before the J^+_{sat} roll-over, followed by D_α emission receding, close to when the roll-over occurs, at around 0.93 s. This behaviour occurs because the electron temperature cools to the point where the concentration of C^{2+} ions is too low to result in a detectable C III emission signal at the camera in the case of CIII emission. The reduction in D_α emission is also thought to be a consequence of low T_e, due to the excitation rate of neutrals decreasing, which also suggests the rate of ionization is low in this region.

The dynamics of movement of C and Balmer emission peaks from the target towards the x-point is informative about the dynamics of detachment. The edge of the C III emission moves at a speed of ~1 m/s in the poloidal direction and ~20 m/s along the

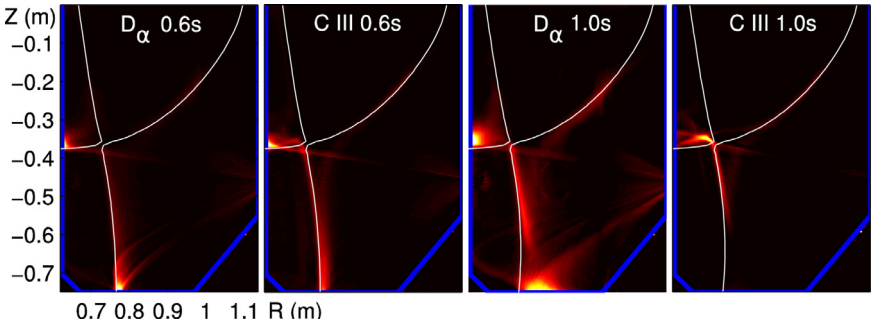

Fig. 4. Poloidal emissivity profiles of D_α and C III emission at 0.6 s (left) and 1.0 s (right) in shot 52,065, at the onset of detachment.

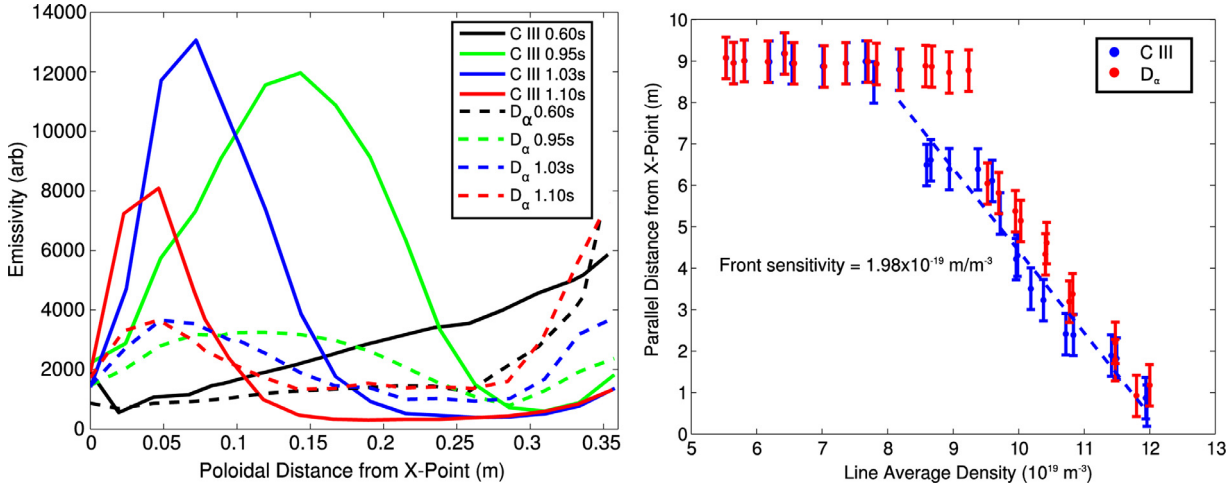

Fig. 5. (left) time evolution of C III (solid lines) and Da emissivity along the outer divertor leg at 3 times in the density ramp, (right) location of the edge of the C III and D_α emitting regions as a function of the line average density in the core plasma.

magnetic field. These speeds are orders of magnitude slower than characteristic velocities in the divertor leg. For comparison, the ion acoustic velocity for T_i=T_e= 1 eV is $\sim 10^4$ m/s. This suggests that this movement is not due to the propagation of an instability, but more likely signifying the transition between stable states during the density ramp [16]. After the C III emission starts to move toward the X-point, two features appear in the D_α emissivity profiles: one peak near the strike point, which interpretive modelling presented in Section 5 suggests is a due to a combination of neutral excitation, ion-electron recombination and molecular dissociation processes, and a second, further up the divertor leg. The second peak approximately tracks the position of the edge of the C III emitting region, as shown in Fig. 5, and appears to be mostly due to neutral excitation as neutrals ionize due to multiple collisions with electrons. The movement of this region is therefore indicative of the ionization source moving toward the X-point as the temperature along the outer leg reduces throughout the density ramp, thereby increasing the ionization mean-free-path of recycled neutrals formed at the outer divertor.

The electron density profile along the outer leg was measured with a multi-channel spectrometer configured to record the intensity and shape of the D_δ (410 nm) and D_ε (398 nm) spectral lines. From these measurements, the electron density was inferred by fitting a convolution of the instrumental broadening with the Stark broadened line shape [17]. These measurements suggest that the peak of the electron density profile remains close to the strike point throughout the density ramp, and does not appear to move toward the X-point at the highest density achieved in the experiment, as observed in other experiments on other devices, such as JET [18], AUG [13], JT-60 U [19] and others.

5. Interpretive modelling

The OSM-EIRENE and DIVIMP codes were used to test the consistency of the data collected from the experiment by using a subset of the data (excluding the measured D_α and D_γ emission lines, which are later used to check the quality of the plasma solution) to constrain the OSM interpretive code that models the deuterium plasma ions and electrons, the EIRENE kinetic neutral transport code is used to model the neutrals arising from recycling at the divertor strike points and gas valves and the DIVIMP kinetic code to calculate the source and transport of carbon impurities through the plasma. The sources of particles and sinks of particles in the plasma arising from ionization and recombination processes respectively are calculated by EIRENE and passed to OSM which solves the particle and momentum conservation equations along field lines. The two codes are then iterated until they reach convergence. The diagnostics (and measured plasma parameters) used to constrain the code include: Thomson scattering measurements (upstream n_e, T_e), Langmuir probes (J^+_{sat} at the inner and outer strike points, n_e and T_e at the attached inner target), inverted C III emission profiles along the outer divertor leg (the location of the cut-off in the emission is assumed to correspond to where T_e ~3 eV) and divertor spectroscopy (n_e at positions long the outer leg derived from the shape of the Stark broadened D_δ and D_ε emission lines described in Section 5) [17,20].

The interpretive simulations were carried out at 3 times in the experiment, at 0.7 s, when the divertor leg is attached, 1.0 s at the peak in the outer strike point J^+_{sat} profile and 1.2 s when the outer leg is detached. The estimates of n_e and T_e at the outer strike point at 0.7 s were used to constrain these parameters in the code, after this time, analysis of the Langmuir probe data suggests T_e ~5 eV, which is inconsistent with the lack of C III emission across nearly half of the divertor leg, as shown in Fig. 5, consistent with previous reports that T_e is likely over-estimated in these experiments [1]. Furthermore, an increase in the ratio of the D_ε/D_δ emission lines is measured during this period, indicating the presence of volumetric recombination processes, which are more likely to occur at lower temperatures, < 2 eV The electron temperature and density profiles along the outer leg used in the interpretive simulations are shown in Fig. 6.

DIVIMP simulations were carried out in order to check the consistency of the constraints that were applied in the OSM code modelling. In the OSM the constraints were applied to mimic the disappearance of C III emission in the outer leg and relied on the inverted camera data from experiments and ADAS calculations of the fractional abundance of the C^{2+} charge state in coronal equilibrium. The more sophisticated DIVIMP simulations, that use a kinetic transport model to simulate the spatial distribution of all carbon charge states, and collisional-radioactive atomic data also from ADAS, provide a means of testing whether the boundary conditions applied in the code are consistent with the data. Cross-field transport of impurities in DIVIMP is modelled as a purely diffusive process, where the specified cross-field diffusion coefficient was set to 1 m^2/s. The forces acting on the impurities, due to temperature gradients, and friction due the flow of deuterium ions, are calculated from the OSM plasma solution. The DIVIMP modelling suggests that at 1 s, as the divertor enters detachment, the main source of carbon in the divertor is due to physical sputtering occurring at the attached inner strike point. The source of carbon at the

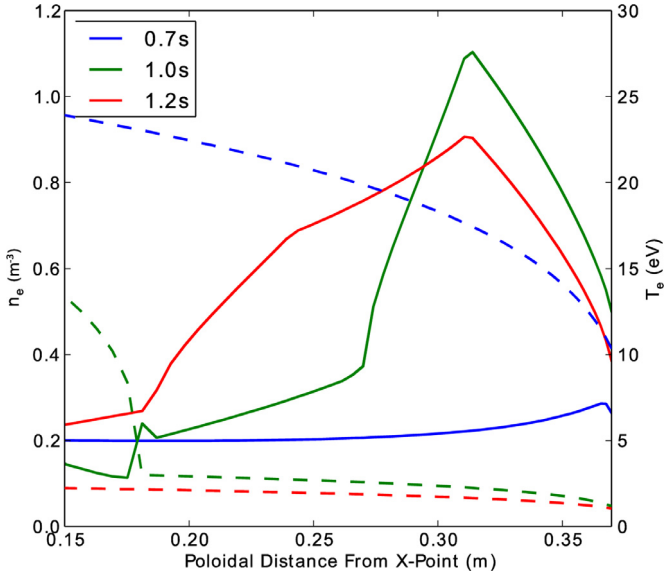

Fig. 6. Profiles of density (solid lines) and electron temperature (dashed lines) along the outer leg at 0.7 (blue), 1.0 (green) and 1.2 s (red). (For interpretation of the references to colour in this figure legend, the reader is referred to the web version of this article.).

outer strike point is purely due to chemical sputtering, and is an order of magnitude lower than the source at the inner strike point. Comparison of the measured C III emissivity profile along the outer leg with that calculated by DIVIMP, shown in Fig. 7, confirm that the boundary condition applied in the code to set T_e ~3 eV where the C III diminishes has had the desired effect.

The consistency of the data from experiments used to constrain the model was tested by comparing the D_γ/D_α line ratio profiles at the three times of interest, and comparing with the ratios measured from the inverted camera measurements. This line ratio is a good check of the quality of the simulations, as it is indicative of the role of recombination compared with excitation (and ionization) in establishing the particle balance in the divertor [21]. The camera data were uncalibrated, so a relative ratio was used where the measured and simulated D_γ/D_α ratios at 0.7 s were scaled by a spatially uniform factor so the average ratio was ~1 along the outer leg. The line ratios at a later time were scaled by the same factors, so the relative change in the line ratios can be compared. The results of these calculations, shown in Fig. 7, show that close to the divertor target, the code under-estimates the D_γ emission compared with experiment, but is generally in reasonable agreement, within a factor of ~2, 5 cm from the strike point. Both the measured and calculated line ratios at 1.0 and 1.2 s exceed 1 in a region close to the strike point that expands up the divertor leg in time. The interpretive simulations suggest this region has low electron temperature (< 3 eV) and high density (up to $\sim 10^{20}$ m^{-3}) that expands up the divertor leg during the density ramp. The particle sink term arising from radioactive, 3-body and molecular activated recombination processes outlined in [22] calculated by EIRENE is found to be small compared with the ion flux entering the divertor leg, which is consistent with spectroscopic estimates of the volume recombination rate.

6. Summary & conclusions

Ohmic density ramp experiments in the single null magnetic configuration were carried out, in which the ion ∇B drift was directed away from the primary X-point. During the density ramp, the outer leg is found to detach, and the inner leg remains attached. A detailed analysis of the data collected from Thomson scattering, Langmuir probes, reciprocating probes, bolometry and filtered cameras is presented, to show the changes in the plasma conditions that occur in the boundary plasma before and after the onset of detachment, defined here to coincide with when the ion flux to the outer divertor strike point starts to decrease. At 0.32 s before the onset of detachment, C III emission starts to recede from the outer strike point toward the X-point, due to the electron temperature reducing throughout the density ramp. At 0.1 s before detachment, the Langmuir probes at the outer strike point suggest the peak density there increases more slowly than the approximately linear trend with upstream density that is evident earlier in the experiment. This is coincident with an expansion of the radial width of the D_α emission at the outer strike point and an increase in the radiation emitted in the outer SOL. At the time when detachment occurs, there is a strong reduction in the electron density at the outer divertor strike point, which is largely responsible for the roll-over in the ion flux. Also, the radiation emitted in the outer leg and inner SOL appears to saturate at the time when the roll-over occurs. In the case of the outer leg, this is due to a contraction in the volume where the radiation is

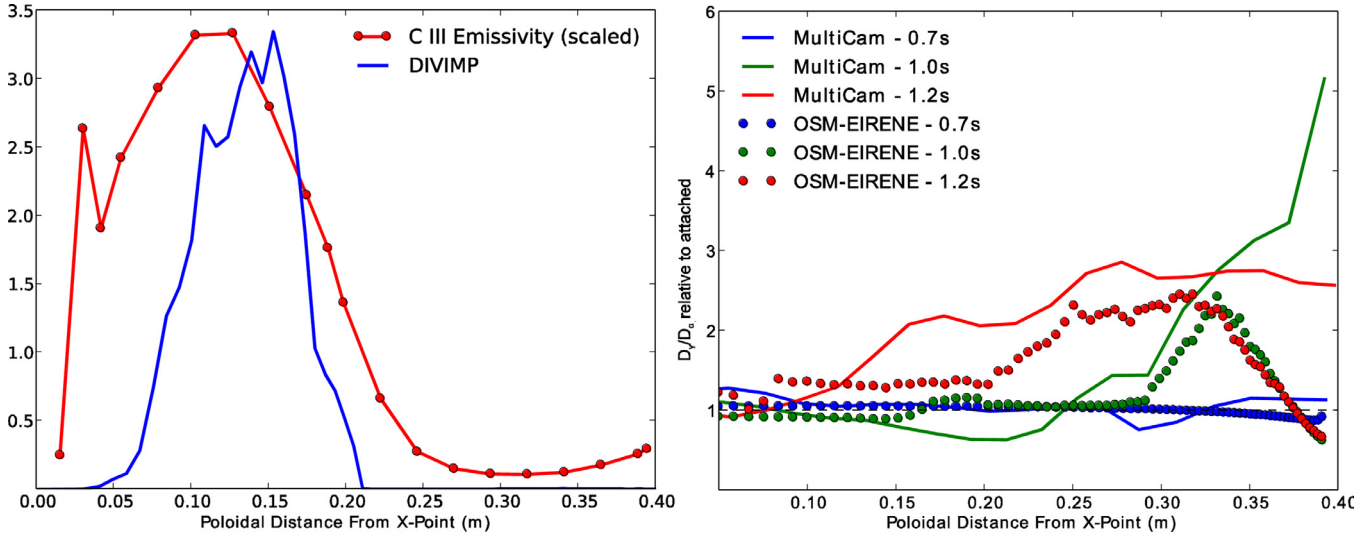

Fig. 7. (left) comparison of measured C III line emissivity along the outer divertor leg measured at 1.0 s with the result from a DIVIMP simulation (right) comparison of measured D_γ/D_α line emissivity ratio profiles with output from OSM-EIRENE simulations.

emitted, and becoming more concentrated near the X-point with a higher emissivity. A broadening of the upstream density profile is also found to occur after the onset of detachment, however more measurements are required to establish when the broadening occurs relative to the onset of detachment.

The consistency of measurements of the plasma conditions in the divertor leg before and after the onset of detachment have been checked with the interpretive OSM-EIRENE DIVIMP suite of codes. Measurements from the Thomson scattering, Langmuir probes, divertor spectroscopy and C III imaging are used as input to the model, and calculating the ratio of the D_γ/D_α Balmer emission lines, to compare with data obtained from the experiment. The calculations confirm the main assumptions that were applied to interpret the C III imaging data, as the C III emissivity distribution calculated by DIVIMP is largely in agreement with measurements. The calculated and measured D_γ/D_α profiles are in reasonable agreement, within a factor of two, with the worst disagreement being within 5 cm of the outer divertor strike point, where the code appears to underestimate the D_γ emissivity. The cause of this discrepancy is under investigation.

The general characteristics of detachment in TCV are similar to that found in higher density tokamaks and there is consistency between model and experiment. Generally, it is found that detachment process develops more slowly than in other, higher density tokamaks. Understanding that difference and its dependence on the underlying processes of detachment (line radiation, in collisions and recombination) will be helpful determining the relative importance of those processes.

Acknowledgement

This work has been carried out within the framework of the EUROfusion Consortium and has received funding from the Euratom Research and Training Programme 2014–2018 under grant agreement No 633053 and from the RCUK Energy Programme [grant number EP/I501045]. To obtain further information on the data and models underlying this paper please contact PublicationsManager@ccfe.ac.uk. The views and opinions expressed herein do not necessarily reflect those of the European Commission.

References

[1] R.A. Pitts, B.P. Duval, A. Loarte, J.-M. Moret, J.A. Boedo, D. Coster, I. Furno, J. Horacek, A.S. Kukushkin, D. Reiter, J. Rommers, J. Nucl. Mater. 290-293 (2001) 940–946.
[2] S.W. Lisgo, J. Nucl. Mater. 337-339 (2005) 256–260.
[3] G.F. Matthews, J. Nucl. Mater. 220-222 (1995) 104–116.
[4] A. Loarte, Nucl. Fusion 38 (1998) 3.
[5] F. Reimold, Nucl. Fusion 55 (2015) 033005.
[6] M. Wischmeier, J. Nucl. Mater. 390-391 (2009) 250–254.
[7] M. Wischmeier, J. Nucl. Mater. 415 (2011) S523–S529.
[8] M. Wischmeier, in: Proc. 32nd EPS conference, Tarragona, 2005 P-5.013.
[9] D.D. Ryutov, Phys. Plasmas 14 (2007) 064502.
[10] P. Valanju, M. Kotschenreuther, S.M. Mahajan, J. Canik, Phys. Plasmas 16 (2009) 056110.
[11] B. LaBombard, Nucl. Fusion 55 (2015) 053020.
[12] P.C. Stangeby, The Plasma Boundary of Magnetic Fusion Devices, 2000.
[13] S. Potzel, M. Wischmeier, M. Bernert, R. Dux, H.W. Müller, A. Scarabosio, Nucl. Fusion 54 (2014) 013001.
[14] D. Carralero, Phys. Rev. Lett. 115 (2015) 215002.
[15] A.H. Andersen, A.C. Kak, Ultrasonic Imaging 6 (1984) 81–94.
[16] B. Lipschultz, F.I. Parra, I.H. Hutchinson, Nucl. Fusion 56 (2016) 056007.
[17] B.A. Lomanowski, A.G. Meigs, R.M. Sharples, M. Stamp, C. Guillemaut, Nucl. Fusion 55 (2015) 123028.
[18] A.G. Meigs, J. Nucl. Mater. 438 (2013) S607–S611.
[19] N. Asakura, J. Nucl. Mater. 241-243 (1997) 559–563.
[20] K. Verhaegh et al., These proceedings.
[21] G.M. McCracken, Nucl. Fusion 38 (1998) 619–629.
[22] J.R. Harrison, PhD thesis (2010).